Low-temperature thermal conductances of amorphous dielectric microbridges in the diffusive to ballistic transition

S. Withington,* D. J. Goldie, and A. V. Velichko
Cavendish Laboratory, JJ Thompson Avenue, Cambridge, United Kingdom
(Received 4 January 2011; revised manuscript received 4 April 2011; published 9 May 2011)

Through a lossy acoustic-wave model we explore the effect of inelastic scattering on the low-temperature thermal conductances of amorphous dielectric microbridges in the diffusive to ballistic transition. The model gives not only the thermal flux as a function of geometry and temperature, but also the temperature distribution of the internal degrees of freedom that constitute the loss, which in turn can be used for calculating noise. The approach leads to powerful conceptual insights and provides a numerical framework for analyzing experimental data. Si_xN_y tends to behave ballistically at low frequencies and diffusively at high frequencies, and when integrated over all frequency, the diffusive to ballistic transition becomes apparent at lengths of around a few hundred microns. It is possible to include flux-dependent acoustic loss, which leads to counterintuitive thermal behavior. A sample can behave diffusively when measured using a small temperature difference, but ballistically when measured using a large temperature difference. There is compelling circumstantial evidence that the effects of acoustic saturation have been seen, but not explicitly recognized, on many occasions.

DOI: 10.1103/PhysRevB.83.195418 PACS number(s): 66.70.Hk, 07.57.Kp, 95.55.Rg, 85.25.Pb

I. INTRODUCTION

The ability to micromachine amorphous dielectric materials into components having scale sizes ranging from hundreds of nanometers to hundreds of microns has led to a wealth of new physics and a host of new technological opportunities. For example, silicon nitride membranes and microbridges are used in applications as diverse as far-infrared and x-ray detectors for astronomy, particle detectors for dark-matter searches, and calorimeters for low-energy surface physics. When designing components for these applications, it is necessary to understand how low-dimensional structures store heat and exchange heat with their surroundings, and more problematically the physical processes that give rise to noise.[1]

The aim of this paper is to consider how acoustic loss influences the low-temperature thermal conductances of amorphous dielectric microbridges, in particular, to study the way in which the thermal conductance G of a sample changes as its length l approaches and becomes smaller than the phonon scattering length. This range is sometimes referred to as the *diffusive to ballistic transition*. The key point is that a long sample has a conductance that scales as $1/l$, whereas a short sample has a conductance that tends to the quantum limit.[2] Often, however, it is necessary to understand the behavior of structures that are intermediate between these two extremes. In fact, a conductor may behave diffusively over one range of phonon energies, but ballistically over another; or diffusively over one part of its length, but ballistically over another. A further issue is that it is sometimes necessary to calculate the thermal noise generated by a microbridge, which in turn requires the temperature to be known as a function of position. These issues become acute when developing ultra-low-noise transition edge sensors for far-infrared space telescopes, where conductances of less than 0.1 pW K^{-1} must be achieved, and where thermal fluctuation noise determines the ultimate sensitivity.[3]

Although there are many publications on the low-temperature thermal properties of low-dimensional structures, they concentrate on samples that are either very long or very short compared with the scattering length.[4] They also assume that the scattering is elastic, and usually attribute it to surface roughness.[5] This approach is valid for crystalline and polycrystalline materials, but it has been known since the 1970s that the low-temperature bulk thermal behavior of amorphous material is very different from that of ordered dielectrics.[6] The thermal and acoustic behavior of amorphous materials is strongly affected by the excitation of low-energy configurational states.[7] More recently it has been observed that the Q factors of micromechanical resonators are strongly influenced by low-energy dissipative mechanisms, some of which may be related to surface contamination and relaxation processes.[8] It seems inevitable, therefore, that the conductances of long amorphous microbridges must be strongly affected, perhaps even dominated, by inelastic scattering even when surface or grain-boundary scattering is present. Despite the likely role of inelastic scattering we are not aware of any publication that discusses, explicitly, the effect of acoustic loss on the heat transport properties of low-dimensional microbridges.

In this paper, we describe a technique for calculating the thermal conductances of structures having significant bulk inelastic scattering. The scattering is introduced as an acoustic loss that can have any functional dependence on temperature and frequency. The model gives not only the heat flux as a function of geometry and temperature, but also the temperature distribution of the internal degrees of freedom that constitute the loss, which in turn can be used for calculating noise. The model reproduces the principal features of heat transport in low-dimensional low-temperature systems, and provides a conceptual framework for understanding the range of behavior seen. It is shown that the saturation of the scattering mechanism, which is a well-known feature of acoustic propagation in amorphous dielectrics,[9] can give rise to counterintuitive thermal behavior. Indeed, there is compelling circumstantial evidence that the effects of saturation have been seen, but not explicitly recognized, on many occasions.

II. BACKGROUND CONSIDERATIONS

Heat is transported in low-dimensional insulating structures at cryogenic temperatures by low-order vibrational modes. In the case of amorphous dielectrics, such as low-stress Si_xN_y, it is beneficial to determine the vibrational behavior through continuum mechanics, because the acoustic phonon modes are well defined even though the material is disordered. Usually it is assumed that the material is perfectly elastic, and the dispersion relationships are found, for a structure of any shape and composition, by solving the wave equation using a generalized eigenvalue routine.[10] Knowledge of the modal forms alone, however, does not allow thermal conductance to be determined apart from in the extreme ballistic limit. To determine thermal conductance, scattering must be introduced, which can be elastic or inelastic. In low-noise applications it is important to distinguish between elastic and inelastic scattering, because elastic scattering does not contribute thermal noise of its own, whereas inelastic scattering does. For example, it would be possible to calculate the harmonic modes of a sample with frozen-in density and edge-profile perturbations, and the high-order eigenvalues would be reduced compared with the defect-free case, indicating a reduced number of effective modes, but the structure would not radiate thermal noise.

In the case of elastic scattering, various models have been proposed to take into account surface roughness,[11] inhomogeneities, and step discontinuities.[12] The influence of surface roughness is usually calculated by scattering plane-wave basis functions, but for low-dimensional structures it is more properly described as a longitudinal spatial variation of the dispersion relationships. Santamore and Cross[11] have calculated the effect of surface roughness on the conductivity of low-dimensional bars, and by assuming a certain spectral form for the roughness correlation function were able to model the results of Schwab.[13] Schwab's measurements were made on a short (<1 μm) length of Si_xN_y, and so the sample should have been operating in the ballistic regime, where surface roughness is likely to be dominant. It is of concern, however, that Santamore and Cross had to invoke a certain periodicity in the roughness correlation function in order to describe what was seen. In a recent paper,[14] the scattering problem is approached in a different way: defects scatter energy into acoustic modes that are cut off by the large-scale dimensions of the sample. The resulting evanescent modes store energy and therefore contribute to the heat capacity. This mechanism must take place at every defect site but still constitutes an elastic process.

In the case of inelastic scattering, the situation is more complicated. Many components are fabricated using amorphous materials such as Si, Si_xN_y, SiO, and SiO_2, which are known to exhibit extreme non-Debye-like thermal behavior.[6,15] The observed anomalies are intimately related to the existence of defects, such as voids, and the stoichiometry of the material, with the incorporation of excess Si or O, or trapped hydrogen left over from the deposition process, being significant. Although the composition and microstructure vary markedly from one material to another, the bulk thermal properties of all glassy materials are remarkably similar. In particular, the heat capacity varies approximately as T, which is believed to indicate the excitation of low-energy configurational states, called two level systems (TLSs).[7] The dielectric properties of amorphous materials are also influenced by the existence of TLSs, with the relationship between the acoustic and dielectric behaviors being dependent on the ionic content of the material.[16,17] Recent theoretical work addresses the problem of how long-wavelength elastic modes interact with TLSs.[18,19] The low-temperature acoustic behavior of amorphous materials has been studied experimentally, and it is known that amorphous materials are highly lossy at ultrasonic and hypersonic frequencies.[20] Moreover, the losses have characteristics indicative of resonant absorption by configuration states.[21,22] Given that the specific heat behaves in an extreme non-Debye-like manner, and that amorphous materials are acoustically lossy, there is no reason to believe that the thermal conductances of long microbridges can be described by a lossless acoustic-wave model with elastic surface scattering. It may be said that when the attenuation length is several times larger than the cross-sectional dimensions, surface scattering becomes the dominant mechanism, but there is a problem because when the sample is much longer than the attenuation length, acoustic loss must still play a key role, even if surface scattering is present.

In recent years, we have measured the conductances of hundreds of Si_xN_y microbridges having different geometries, at different temperatures and in different ways.[23–26] Other groups have carried out similar work.[27–30] The heat flux I through a sample having end temperatures T_c and T_h can be described to high accuracy, over restricted temperature ranges, through an expression of the form $I = k[T_h^n - T_c^n]$, where k and n are numerically derived parameters. It is very difficult, however, to come up with a single physical model that can account for all of the results across a wide range of temperatures and geometries, because each time some aspect of an experiment is changed, the derived parameters imply a different regime of operation. Here are some examples:

(i) We have measured many Si_xN_y microbridges, on transition edge sensors, having widths in the range of 3–30 μm, lengths in the range 100–400 μm, and thicknesses of 0.5 μm. All of the exponents are in the range $n = 2.8$–3.1 at temperatures from 300 to 800 mK.[23] Many of the devices should be operating as three-dimensional (3D) conductors, and yet the exponent is always significantly smaller than 3D ballistic transport would suggest. The results are, however, characteristic of the bulk behavior of amorphous materials.

(ii) Early low-temperature measurements made by a number of groups[31] on Si_xN_y show $n \approx 3.6$, which is not consistent with the expected properties of amorphous materials.

(iii) We have measured the specific heat of the Si_xN_y used for our own devices, and it scales linearly with temperature,[24] which is characteristic of the resonant excitation of TLSs and not at all characteristic of Debye-like behavior.

(iv) When measuring samples having widths in the range 1–4 μm, lengths in the range 150–950 μm, and thicknesses of 0.2 μm, operating at temperatures of around 100 mK, we find that the exponent is in the range $n = 1.2$–2.4, which is characteristic of highly scattered low-dimensional transport.[26] Similar structures, however, made from the same material, show $n > 3.5$ at temperatures above 1 K, implying near-ballistic 3D transport.[32]

(v) An elastic scattering mechanism having a scale length that can cause appreciable scattering at low temperatures, <0.1 K, can only become more significant at high temperatures, >0.8 K, which is similar to the problem of Santamore and Cross.[11]

(vi) Using atomic force microscopy, we have measured the surface roughnesses of samples (<10 nm) and cannot account for the level of low-temperature scattering seen.

(vii) Notionally identical samples having a thickness of 0.5 μm show thermal conductance variations of around $\pm 5\%$, which cannot be accounted for by the variation in measured surface roughness. Samples having a thickness of 0.2 μm show thermal conductance variations of around $\pm 10\%$, which might suggest that surface scattering or bulk defects are influencing behavior.

(viii) We have measured, using a differential technique, the conductance of a sample measuring 10 μm wide, 500 μm long, and 0.5 μm thick, and find that $n = 1.8$ at 270 mK, changing smoothly to $n = 3.6$ at 1.5 K.[32] Higher-conductance structures on the same chip, measured using a nondifferential technique, give $n = 2.2$ at 270 mK, and $n = 3.6$ at 1.5 K. At low temperatures, the exponent seems to depend on the way in which the measurement is performed.

(ix) The conductances of some samples show a reciprocal dependence on length; but at higher temperatures, seemingly identical structures have a different dependency. Overall, these observations strike an accord with the comments of Cross and Lifshitz[12] who point out that the vibrational modes of mesoscopic systems have anomalously low Q values compared with larger systems of the same material. They also remark that unexpected dependencies on temperature and magnetic field have been observed and remain unexplained.

Taken together these observations suggest that heat is transported in low-dimensional amorphous structures in more complicated ways than models based on the surface elastic scattering of low-order phonon modes would suggest.

III. INFINITELY LONG CONDUCTORS

To begin, it is beneficial to emphasize the relationship between the acoustic properties of a microbridge and its thermal behavior. At low temperature, 100 mK, and high frequency, 1 GHz, the acoustic attenuation in amorphous dielectrics is around 10 dB mm^{-1}, rising steeply with frequency.[33,34] The width of a typical microbridge, <100 μm, is smaller then the attenuation length, which shows that, at low frequencies, there must be a high degree of coherence across the sample. At high frequencies, say 100 GHz, this condition is only satisfied for narrow bridges, <1 μm. Moreover, for a wave model to be applicable, the attenuation length must be larger than the wavelength. Assuming a maximum sound speed of 10 km s^{-1}, the attenuation per wavelength is 0.1 dB, which means that at low frequencies phonons travel on average 100 wavelengths before being absorbed. This rough calculation suggests that a damped acoustic-wave model is appropriate for describing the thermal behavior of Si_xN_y microbridges, but it should be recognized that a sample may behave ballistically over one range of phonon energies, but diffusively over another.

The simplest analysis of conductance is based on a model where wave packets travel ballistically between regions where complete thermalization takes place, but in reality the transfer of energy to internal degrees of freedom is a distributed process. Represent a thermal conductor as an infinitely long acoustic transmission line, comprising a chain of lossy elements each of which has a power transmission factor of α, and a length Δx. The lossy elements reradiate energy in each direction at a rate of $(1-\alpha)F_j$, where F_j is the spectral density of the thermal flux associated with a source having temperature T_j. It can be shown, through an iterative process, that the *net* flux spectral density traveling to the right at reference plane j is given by

$$q_j = -(1-\alpha)\sum_{k=0}^{\infty}\alpha^k[F_{j+k+1} - F_{j-k}], \tag{1}$$

where the first and second terms come from sources to the left and right of plane j, respectively. Assuming that we are only interested in the behavior of a small part of the sample, which is how conductance is defined, then the source flux can be expanded linearly with position, and

$$\begin{aligned} F_{j+k+1} &= F_0 + (j+k+1)\Delta x\frac{\partial F}{\partial x}, \\ F_{j-k} &= F_0 + (j-k)\Delta x\frac{\partial F}{\partial x}. \end{aligned} \tag{2}$$

Using Eqs. (1) and (2),

$$q = -(1-\alpha)\sum_{k=0}^{\infty}\alpha^k(1+2k)\Delta x\frac{\partial F}{\partial x}. \tag{3}$$

As would be expected for an infinitely long sample with sources that depend linearly on position, the flux is independent of position, which is a requirement of thermal equilibrium.

D'Alembert's ratio test shows that the series converges for $\alpha < 1$. Also,

$$(1-\alpha)\sum_{k=0}^{\infty}\alpha^k(1+2k) = (1-\alpha)\left[\sum_{k=0}^{\infty}\alpha^k + 2\sum_{k=0}^{\infty}k\alpha^k\right]. \tag{4}$$

The first term on the right-hand side (RHS) is the sum of a geometric progression, and therefore Eq. (4) can be written

$$(1-\alpha)\left[\frac{1}{1-\alpha} + 2\sum_{k=0}^{\infty}k\alpha^k\right] = \left[\frac{1+\alpha}{1-\alpha}\right]. \tag{5}$$

The flux becomes

$$q = -\left[\frac{1+\alpha}{1-\alpha}\right]\Delta x\frac{\partial F}{\partial x}, \tag{6}$$

but this flux corresponds to a quasimonochromatic traveling wave. Introducing the Planck function $U(T)$ for the thermal sources,

$$U(T) = \frac{1}{e^{\hbar\omega/k_BT} - 1}, \tag{7}$$

and integrating over all frequencies leads to

$$I = -\frac{1}{2\pi}\int_{\Omega}^{\infty}\hbar\omega\frac{\partial U}{\partial x}\left[\frac{1+\alpha}{1-\alpha}\right]\Delta x\, d\omega, \tag{8}$$

where Ω is the cutoff frequency of the mode. Finally, for a number of modes, and introducing the temperature gradient,

$$I = \underbrace{\frac{1}{2\pi}\sum_m \int_{\Omega_m}^{\infty} \hbar\omega \frac{\partial U}{\partial T}\left[\frac{1+\alpha}{1-\alpha}\right]\Delta x\, d\omega}_{G}\left(-\frac{\partial T}{\partial x}\right). \quad (9)$$

where α is generally a function of frequency, and depends on mode number. We are assuming that the overall conductance is given by the parallel combination of the conductances of the individual modes, which need not be true. Also, we are assuming that the reradiation is thermal, but the thermalizing mechanism is not known. The coupling of TLSs by localized phonon modes[35] is a strong possibility.

Equation (9) is identical to the usual expression for thermal conductance G, but with the actual scattering length replaced by an effective scattering length

$$l_{\text{eff}} = \left[\frac{1+\alpha}{1-\alpha}\right]\Delta x. \quad (10)$$

Equation (10) takes into account that although the absorption of power is associated with some scattering length, a fraction α of the phonons remains unscattered after propagating through a distance Δx.

For lossy material, the power in a mode decays as $\eta = \alpha^{(l/\Delta x)}$, where η is the total power transmission efficiency of a sample of length l, and therefore $l = [\ln(\eta)/\ln(\alpha)]\Delta x$. For $\alpha > 0.3$, to an exceedingly good approximation, which improves as α approaches unity,

$$\left[\frac{1+\alpha}{1-\alpha}\right]\Delta x \approx \frac{-2}{\ln(\alpha)}\Delta x = \frac{-2l}{\ln(\eta)} = \gamma; \quad (11)$$

in the last step we have assumed that the power in a mode decays according to $\eta = \exp(-2\,l/\gamma)$, where γ is the acoustic attenuation length. It is clear that the scattering length that appears in the usual expression for thermal conductance is the distance over which the amplitude of the acoustic wave decays to $1/e$ of its original value, which is reasonable because the parameter of most physical significance is the phase coherence length, rather than the scattering length itself. Using Eq. (11) in Eq. (9) gives

$$I = \underbrace{\frac{1}{2\pi}\sum_m \int_{\Omega_m}^{\infty} \hbar\omega \frac{\partial U}{\partial T}\gamma\, d\omega}_{G}\left(-\frac{\partial T}{\partial x}\right). \quad (12)$$

Thus, a simple lossy acoustic transmission-line model reproduces the classical expression for thermal conductance.

IV. FINITE-LENGTH CONDUCTORS

To understand how conductance approaches the quantum limit, we must consider finite-length conductors. It is possible to extend the scheme described in Sec. III to take into account the terminations, but in this case the resulting system of linear equations must be solved through matrix inversion. All of our early simulations were carried out in this way. This linear approach does not, however, allow the attenuation to be a function of temperature, and therefore, initially, an unknown function of position. To allow general functional dependencies, we adopt a nonlinear approach.

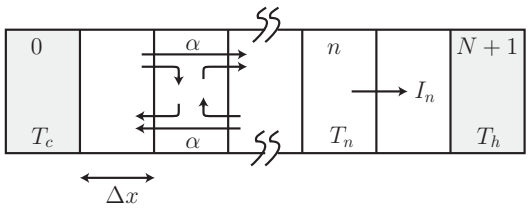

FIG. 1. (Color online) Divide the conductor into N cells of length Δx: $\{n \in 1,\ldots,N\}$. The terminations have cold and hot temperatures T_c and T_h, corresponding to $n = 0$ and $n = N+1$, respectively. Each cell has a power transmission efficiency of α, which is generally a function of temperature and frequency, $\alpha(T_n,\omega)$, and reradiates power with an efficiency $(1-\alpha)$. The net thermal flux passing to the right through reference plane n is I_n.

Divide the structure, Fig. 1, into cells of length Δx, and label the cells 1 to N. The two heat baths, 0 and $N+1$, are perfectly absorptive, and they are held at known, fixed temperatures $T_0 = T_c$ and $T_{N+1} = T_h$. At each cell, an incident acoustic wave is transmitted with a power transmission factor of α, and absorbed with a factor $1-\alpha$. Each cell reradiates acoustic energy, and the radiated wave is phase incoherent with respect to the incoming wave. According to this model, the *total* flux I_n traveling to the right across reference plane n is given by

$$\begin{aligned} I_n = &\sum_{j=1}^{n}\sum_m \frac{1}{2\pi}\int_{\Omega_m}^{\infty} \hbar\omega\, U(T_j)[1-\alpha^m(T_j,\omega)]\beta_{jn}^m(\omega)\, d\omega \\ &- \sum_{j=n+1}^{N}\sum_m \frac{1}{2\pi}\int_{\Omega_m}^{\infty} \hbar\omega\, U(T_j)[1-\alpha^m(T_j,\omega)]\beta_{n,j-1}^m(\omega)\, d\omega \\ &+ \sum_m \frac{1}{2\pi}\int_{\Omega_m}^{\infty} \hbar\omega\, U(T_0)\beta_{0n}^m(\omega)\, d\omega \\ &- \sum_m \frac{1}{2\pi}\int_{\Omega_m}^{\infty} \hbar\omega\, U(T_{N+1})\beta_{nN}^m(\omega)\, d\omega, \end{aligned} \quad (13)$$

where $\alpha^m(T_j,\omega)$ is the acoustic power transmission factor of cell j in mode m, which may be a function of frequency ω, and $\beta_{rs}^m(\omega)$ is the total acoustic transmission of mode m between reference planes r and s. It is also possible to make the acoustic loss a direct function of position, $\alpha^m(T_j,\omega,x)$, but we shall not do so here. The first term on the RHS of Eq. (13) is the flux traveling to the right from all internal sources to the left of reference plane n, and the second term is the total flux traveling to the left from all internal sources to the right of reference plane n; the third and and fourth terms correspond to the fluxes radiated by the terminations. The first term makes no contribution when $n = 0$, and the second term makes no contribution when $n = N$. The flux includes all modes and has been integrated over all frequency, taking into account the mode cutoff frequencies Ω_m. The system comes into equilibrium when the net fluxes into and out of every cell are equal, $I = I_n\ \forall\ n$.

In situations where the loss is temperature independent, such that it does not depend on position either,

$$\beta_{rs}^m(\omega) = e^{-2(s-r)\Delta x/\gamma_m}. \quad (14)$$

Frequency dependence of γ_m is allowed, but not shown explicitly. Substituting Eq. (14) into Eq. (13) gives

$$\begin{aligned} I = &\sum_{j=1}^{n}\sum_{m}\frac{1}{2\pi}\int_{\Omega_m}^{\infty}\hbar\omega\,U(T_j)(1-e^{-2\Delta x/\gamma_m})\,e^{-2(n-j)\Delta x/\gamma_m}d\omega \\ &-\sum_{j=n+1}^{N}\sum_{m}\frac{1}{2\pi}\int_{\Omega_m}^{\infty}\hbar\omega\,U(T_j)(1-e^{-2\Delta x/\gamma_m}) \\ &\times e^{-2(j-n-1)\Delta x/\gamma_m}d\omega \\ &+\sum_{m}\frac{1}{2\pi}\int_{\Omega_m}^{\infty}\hbar\omega\,U(T_0)e^{-2n\Delta x/\gamma_m}d\omega \\ &-\sum_{m}\frac{1}{2\pi}\int_{\Omega_m}^{\infty}\hbar\omega\,U(T_{N+1})e^{-2(N-n)\Delta x/\gamma_m}d\omega. \end{aligned} \tag{15}$$

If the loss is, additionally, independent of frequency, the temperature can be found as a function of position by evaluating the integrals analytically, and using matrix inversion to solve the resulting system of equations. For a 50-cell system, 50 integral equations having the form of Eq. (15) have to be solved simultaneously.

The functional forms of certain loss mechanisms are known. For example, it is widely believed that acoustic loss in amorphous materials at low temperatures is caused by resonant absorption by TLSs. In this case, the inverse acoustic attenuation length $1/\gamma_m(T_k,\omega)$ is given by[21]

$$\frac{1}{\gamma_m(T_k,\omega)} = \frac{\pi S M^2}{\rho v^3}\omega\tanh\left[\frac{\hbar\omega}{2k_B T_k}\right], \tag{16}$$

where S is the number density of interacting two-level systems, M is the linear coupling between a tunneling state and the strain field, ρ is the mass density, and v is the sound phase velocity. Converting decay length to attenuation using $\eta^m(T_k,\omega) = 8.68/\gamma_m(T_k,\omega)$, we can write

$$\eta^m(T_k,\omega) = \xi\omega\tanh\left[\frac{\hbar\omega}{2k_B T_k}\right], \tag{17}$$

where ξ is the intrinsic attenuation in dB m^{-1} GHz^{-1} at low temperature, $T\to 0$. It has a typical value of 10^4 dB m^{-1} GHz^{-1}. For phonon energies small compared with kT, a few GHz at 200 mK,

$$\eta^m(T_k,\omega) \approx \frac{\xi\hbar\omega^2}{2k_B T_k}. \tag{18}$$

At any given temperature, therefore, the loss increases initially as ω^2 and then as ω. Resonant absorption by TLSs also has the feature that the acoustic loss decreases as the amplitude of the wave increases. Similar behavior is seen in the electric properties of amorphous materials, where the dielectric loss decreases as the electric field increases. Indeed, there seems to be an intimate relationship between the saturation of acoustic loss and dielectric loss.[36,37] Saturation of the loss mechanism can be described by including an additional factor in Eq. (16)

$$\frac{1}{\gamma_m(T_k,\omega)} = \frac{\pi S M^2}{\rho v^3}\omega\tanh\left[\frac{\hbar\omega}{2k_B T_k}\right]\frac{1}{[1+(J/J_s)]} \tag{19}$$

where J is the intensity of the acoustic field, in W m^{-2}, and J_s the value at which saturation occurs.

The actual properties of materials are generally more complicated than Eq. (19) implies, and therefore it is desirable to have a parametric form that can represent measured dependencies. To this end, the power attenuation factor of cell j, at temperature T_j, can be written

$$\eta^m(T_j,\omega,I) = \eta^m(T_c,\omega_c)\left(\frac{T_j}{T_c}\right)^a\left(\frac{\omega}{\omega_c}\right)^b\frac{1}{[1+(I/I_s)^c]}, \tag{20}$$

where a and b are parameters of the model. The last factor in Eq. (20) allows for saturation, where I is the thermal flux, I_s the flux at which saturation occurs, and c a parameter that controls the rate of saturation. $\eta^m(T_c,\omega_c)$ is, therefore, the loss in dB m^{-1} of mode m, at reference temperature T_c, reference frequency ω_c, and low flux levels $I \ll I_s$. In contrast to Eq. (19), the saturation process has been described in terms of thermal flux, in W, rather than acoustic intensity, in W m^{-2}. Although the relationship between the two is not straightforward for low-dimensional systems, Eq. (20) is sufficient for our purposes. $c = 1$ is found to fit measurements of acoustic loss in amorphous dielectrics particularly well: see Fig. 1 of Golding.[33]

Knowing the attenuation factor it is possible to calculate the total transmission, $\beta^m_{rs}(\omega)$ between any two reference planes, $s \geqslant r$:

$$\beta^m_{rs}(\omega) = \begin{cases} 1 & \text{for } r = s \\ 10^{-\frac{\Delta x}{10}\sum_{k=r+1}^{s}\eta^m(T_k,\omega)} & \text{for } r \neq s \end{cases}. \tag{21}$$

Equations (13) and (15) are based on a model where the cut-off frequencies of the individual modes are known. In the case of structures having cross-sectional dimensions that are comparable with the dominant wavelengths, the detailed forms of the modes can be calculated, and Eq. (13) can be used to great effect. For large structures, it is beneficial to represent the number of propagating modes as a continuous distribution. If the loss is the same for all modes, $\beta^m_{rs}(\omega) = \beta_{rs}(\omega), \forall\, m$, and $N(\omega)$ is the number of modes that can propagate at frequency ω, then Eq. (13) becomes

$$\begin{aligned} I = &\sum_{j=1}^{n}\frac{1}{2\pi}\int_{0}^{\infty}\hbar\omega\,U(T_j)[1-\alpha(T_j,\omega)]\beta_{jn}(\omega)N(\omega)\,d\omega \\ &-\sum_{j=n+1}^{N}\frac{1}{2\pi}\int_{0}^{\infty}\hbar\omega\,U(T_j)[1-\alpha(T_j,\omega)]\beta_{n,j-1}(\omega)N(\omega)\,d\omega \\ &+\frac{1}{2\pi}\int_{0}^{\infty}\hbar\omega\,U(T_0)\beta_{0n}(\omega)N(\omega)\,d\omega \\ &-\frac{1}{2\pi}\int_{0}^{\infty}\hbar\omega\,U(T_{N+1})\beta_{nN}(\omega)N(\omega)\,d\omega. \end{aligned} \tag{22}$$

For later use we need to define what is meant by the dimensionality of a microbridge. For a rectangular bar where *both* cross-sectional dimensions are large compared with the wavelengths of significance, we shall say that the conduction is 3D. In this case, it is convenient to use

$$N(\omega) = \frac{wt}{4\pi}\left(\frac{2}{c_t^2}+\frac{1}{c_l^2}\right)\omega^2 + 4, \tag{23}$$

where w and t are the width and thickness of the bar, and c_t and c_l are the transverse and longitudinal sound speeds, which for Si_xN_y are taken to be 6.2 and 10.3 km s^{-1}, respectively. The additional four modes correspond to those that are not cut off at zero frequency. For a rectangular bar where *one* cross-sectional dimension is large compared with the wavelengths of significance, and the other smaller, we shall say that the conduction is two dimensional (2D). In this case,

$$N(\omega) = \frac{w}{\pi}\left(\frac{2}{c_t} + \frac{1}{c_l}\right)\omega + 4. \tag{24}$$

Finally, for a rectangular bar where *both* cross-sectional dimensions are small compared with the wavelengths of significance, we shall say that the conduction is one dimensional (1D), and in this case, $N(\omega) = 4$. It is possible to gain a rough understanding of the temperatures at which the transport changes dimensionality by calculating the temperatures at which the shortest wavelengths present in the Planck spectrum become comparable to the dimensions of the cross section. In other words, none of the wavelengths present in the Planck spectrum are able to propagate. We shall use

$$T_{3D-2D} = \frac{hc_t}{\pi k_B t}, \quad T_{2D-1D} = \frac{hc_t}{\pi k_B w}, \tag{25}$$

where k_B is Boltzmann's constant. For a microbridge having $w = 1.0$ μm and $t = 0.2$ μm, we find $T_{3D-2D} = 470$ mK and $T_{2D-1D} = 95$ mK. It is apparent that when frequency-dependent acoustic loss is present, the excitation spectrum will change, and the threshold temperatures will be pushed to higher values.

Equations (13), (15), and (22) are all systems of $N + 1$ equations (one for each plane, $n \in 0 \cdots N$) in $N + 1$ unknowns (I and the T_j's). The challenge is to find I and the T_j's knowing the properties of the structure, and the temperatures of the terminations. One is left with having to find the solution of a large set of simultaneous nonlinear equations. To this end, note that any one of Eqs. (13), (15), and (22) can be written in the form

$$\mathbf{s}_0(I) - \mathbf{s}_1(\mathbf{t}) + \mathbf{s}_2(\mathbf{t}) = \mathbf{s}_3(T_o) - \mathbf{s}_4(T_{N+1}), \tag{26}$$

where the terms in Eq. (26) correspond directly to the terms in the system of equations to be solved. $\mathbf{s}_0$ is an $(N + 1)$-dimensional column vector having equal entries of I, because in the steady state the flux at every plane is the same. $\mathbf{t}$ is a column vector containing the N unknown cell temperatures, and $\mathbf{s}_3$ and $\mathbf{s}_4$ combine to form a single vector describing the terminations. For any general I and $\mathbf{t}$, the two sides of Eq. (26) will not equate, and we should write

$$\mathbf{\Delta}(\mathbf{x}) = \mathbf{s}_0(I) - \mathbf{s}_1(\mathbf{t}) + \mathbf{s}_2(\mathbf{t}) - \mathbf{s}_3(T_o) + \mathbf{s}_4(T_{N+1}), \tag{27}$$

where $\mathbf{\Delta}(\mathbf{x})$ is an error vector, which is a function of the unknown state vector $\mathbf{x}$. We have included I and $\mathbf{t}$ into a single vector called $\mathbf{x}$. $\mathbf{\Delta}(\mathbf{x})$ is a vector of dimension $N + 1$, where each entry is a nonlinear function of the $(N + 1)$-dimensional state vector $\mathbf{x}$. This function has the same number of equations as unknowns, and thus in principle can be solved, although its conditioning is not known. It is necessary to search for the $\mathbf{x}$ that reduces the error vector to zero, which can be achieved through the iterative procedure

$$\mathbf{x}^{k+1} = \mathbf{x}^k - \chi\left[\mathbf{J}(\mathbf{x}^k)\right]^{-1}\mathbf{\Delta}(\mathbf{x}^k), \tag{28}$$

where χ is a convergence parameter between zero and unity, typically 0.8; although its actual value does not change the result, just the speed and stability of convergence. The elements of the Jacobian $\mathbf{J}(\mathbf{x})$ are the rates of change of the elements of the error vector $\mathbf{\Delta}(\mathbf{x})$ with respect to the elements of the state vector $\mathbf{x}$. The sequence (28) has a quadratic rate of convergence near solution, and is highly efficient. The only remaining question is what temperature distribution $\mathbf{t}$, and what flux I, should be used as the starting guess? Often it is sufficient to start by assuming that all quantities are zero, or that the temperatures are distributed linearly between the two end temperatures. When calculating a series of simulations, say when sweeping one of the end temperatures, it is beneficial to use the solution of the previous calculation as the starting point of the next calculation. In all of the simulations carried out, high accuracy was achieved in 5–10 iterations.

V. SIMULATIONS OF HEAT TRANSPORT

Simulations were carried out using the nonlinear theory described in Sec. IV, and compared, where possible, with the linearized scheme based on matrix inversion. The two agreed precisely in the appropriate limits, and so here we only present results of the nonlinear model.

Using Eqs. (20)–(22), temperature distributions were calculated for a 50-cell, single-mode $N(\omega) = 1$ system. The attenuation factor $\eta(T_k,\omega)$ was made temperature and frequency independent, $a = 0$ and $b = 0$, and I_s was set to an artificially high value to eliminate saturation. The terminations were held at $T_h = 400$ mK and $T_c = 100$ mK. The iteration sequence of Eq. (28) was initiated by assuming zero flux, and cell temperatures equal to the average of the two end temperatures, $(T_h + T_c)/2$. In every case studied, the algorithm achieved the target errors of 1 fW and 1 mK in fewer than 10 iterations, usually only 5. The results are shown in Fig. 2, where attenuation factors of $\eta = 6.02, 0.97, 0.46, 0.22$, and 4.3×10^{-6} dB per cell were used. The length of a sample measured in acoustic attenuation lengths is $L_\gamma = L/\gamma = N\eta/8.68$, where η is the power loss in dB per cell. For the curves shown in Fig. 2, $L_\gamma \approx 35$, 6, 3, 1, and 0, and therefore, at one extreme, the structure is acoustically opaque, $N\eta = 301$ dB, whereas at the other it is acoustically transparent, $N\eta = 2 \times 10^{-4}$ dB. In the opaque case, energy is only exchanged directly between nearest neighbors, but nevertheless significant flux flows through a *diffusive* process. In the transparent case, acoustic waves travel unimpeded along the whole length of the structure, and energy flows through a *ballistic* process. A number of features can be seen in Fig. 2. In the ballistic case, $\eta = 4.3 \times 10^{-6}$ dB, the temperature is independent of position because the internal degrees of freedom are only lightly coupled to the counterpropagating acoustic waves. Moreover, the equilibrium temperature is not the average of the two end temperatures because the total powers radiated by the terminations are not linearly proportional to temperature. In general, it is necessary to distinguish between the temperature of the loss at some position, and the effective temperatures

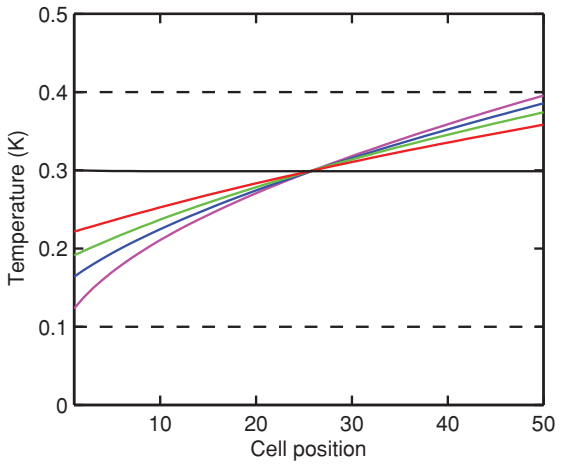

FIG. 2. (Color online) Temperature distributions of single-mode bars terminated at 0.1 and 0.4 K (shown dashed). The power attenuation factors (top to bottom on the RHS) are 6.02, 0.97, 0.46, 0.22, and 4.3×10^{-6} dB per cell. The corresponding heat fluxes were found to be 2, 9, 16, 26, and 58 fW, respectively.

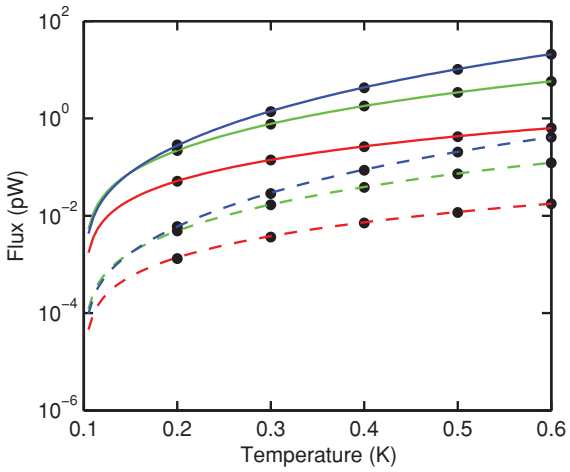

FIG. 3. (Color online) Solid lines show the heat flux as a function of hot temperature T_h for the case where the sample is nearly perfectly acoustically transmissive. $T_c = 0.1$ K. The plots, from top to bottom, correspond to 3D, 2D, and 1D transport, respectively. The filled circles show simulated points, and the solid lines the power-law model described in the text. Dashed lines show the same simulations, but including TLSs having an attenuation factor of $\xi = 6.02$ dB GHz^{-1} per cell.

of the two counterpropagating acoustic radiation fields at the same position; in the ballistic case, these are the three horizontal lines shown in Fig. 2. In the diffusive cases, say $\eta = 6.02$ dB, the temperature varies, essentially, as the square root of position, because the source fluxes radiated by the individual cells are linearly dependent on position, but quadratically dependent on temperature.

In all cases, there is a temperature discontinuity at each end, because the terminations are perfectly acoustically opaque, and the temperature has to change infinitely fast in accordance with the infinitely high thermal impedance. Jumps in temperature at boundaries are also seen in electromagnetic calculations of radiative heat transfer through absorbing material between black parallel plates,[38] and in Monte Carlo simulations[39] of phonon radiative heat transfer in crystalline dielectrics at low temperatures. In real structures, the acoustic transmission of the terminations is finite, the thermal impedance is finite, and the temperature changes over some finite distance. The model indicates correctly that there is always some ambiguity as to what is meant by the *length* of a structure and the *temperatures* of the terminations. Some distance is needed over which the radiation field comes into equilibrium with the internal degrees of freedom that constitute the source and sink. It would be possible to incorporate this effect into the model by distributing the terminations across a number of cells, but we shall not do so here. Many of the features seen in our simulations are also seen when the Boltzmann transport equation is applied to phonon radiative transfer in ballistic and diffusive systems,[40,41] and it is pleasing that the model described here reproduces the behavior of more complex calculations in a way that is straightforward and conceptually appealing. In fact, it seems that our technique, where the overall flux is divided into ballistic and scattered parts, is in close correspondence with the ballistic-diffusive heat transport equations presented by Chen[42,43] for general three-dimensional problems, where the discontinuity is discussed in terms of the injected flux being a boundary condition.

Now consider how the heat flux changes as one of the termination temperatures is varied. Figure 3 shows, as solid lines, the calculated flux for a sample having $w = 2$ μm and $t = 0.5$ μm as a function of T_h when T_c was held constant at 0.1 K. Fifty cells were used, and the attenuation factor was set to 4.3×10^{-6} dB per cell to ensure acoustic transparency at all temperatures and frequencies. The top three plots correspond to perfect 3D, 2D, and 1D heat transport as described by Eqs. (23) and (24). If it is assumed that Si_xN_y has an attenuation factor of typically 10 dB mm^{-1}, then $l = 21.5$ nm, which is unrealistically short, but ensures that the sample is operating in the extreme ballistic limit.

In experimental work, it is common to characterize the heat flux I and differential thermal conductance G through $I = k(T_h^n - T_c^n)$ and $G = knT_h^{n-1}$, respectively. For each of the cases shown in Fig. 3, we derived fits to the simulated data. Only five points were used in each case, because the parameters change very little even when many more points are used. For the ballistic cases we found (3D) $k = 151.0$, $n = 3.87$; (2D) $k = 25.0$, $n = 2.85$; (1D) $k = 1.85$, $n = 2.05$; where k is measured in pW K^{-n}. The 3D case effectively corresponds to ballistic heat transport between two semi-infinite transverse planes, or equivalently ballistic transport along a sample having specularly reflecting surfaces. In this case, the radiated power per unit area is given by $P_{\rm rad} = \sigma(T_h^4 - T_c^4)$, where $\sigma = 157$ W m^{-2} K^{-4} is the Stefan Boltzmann constant for one longitudinal and two transverse modes.[31] On the basis of the dimensions, we would expect $k = 157$ and $n = 4$, which are close to the observed values. The quantum-limited conductance of a single mode is given by $G_q = \pi^2 k_B^2 T/(3h)$, and therefore for a four-mode sample we would expect $k = 1.89$ and $n = 2$, which agrees with the 1D parameters derived. The slight difference is due to the fact that our simulations were not differential calculations as a function of temperature,

but based on the heat flux when one termination was held constant at 0.1 K.

The simple numerical transmission line model correctly reproduces the 3D and 1D ballistic limits, and therefore it is reasonable to expect that it can give a good account of behavior when loss is present. The dashed lines in Fig. 3 show the same simulations as the solid lines but when TLSs having an attenuation factor of $\xi = 6.02$ dB GHz^{-1} per cell were included; Eq. (17) was used to calculate the loss. Once again, the three plots correspond to 3D, 2D, and 1D heat transport, giving (3D) $k = 2.840$, $n = 3.78$; (2D) $k = 0.518$, $n = 2.8$; (1D) $k = 0.053$, $n = 2.1$. Notice that the exponents are essentially unchanged, but the fluxes are reduced by a factor of about 100. It seems that the exponent alone cannot be used to indicate unambiguously whether heat is transported ballistically or diffusively. There can be a significant amount of inelastic scattering, which reduces the flux without changing the exponent.

Figure 4 shows the temperature distributions of 1D microbridges when Eq. (17) was used to include the effects of TLSs, and $\xi = 6.02$, 0.1, 0.01, and 4.3×10^{-6} dB GHz^{-1}. The resulting fluxes were 30 fW, 199 fW, 787 fW, and 1.49 pW, respectively. From a numerical point of view, Fig. 4 demonstrates that the algorithm is quite able to calculate behavior even when the loss is a function of frequency and temperature, and therefore, at the outset, an unknown function of position. From a physical point of view, Fig. 4 has a number of features. For the nearly lossless case, the TLSs are largely decoupled from the counterpropagating radiation fields, but because there are now four modes lightly coupling the losses to the terminations, the internal degrees of freedom come into equilibrium at a slightly higher temperature than those of Fig. 2. Also, when considered along side Fig. 3, it is seen that the temperature distributions associated with 1D ballistic and 1D diffusive behavior are fundamentally different, even though the derived exponents n are very similar. In reality a structure will tend to behave ballistically at long wavelengths and diffusively at short wavelengths, and in some cases ballistically over certain parts of its length and diffusively over others.

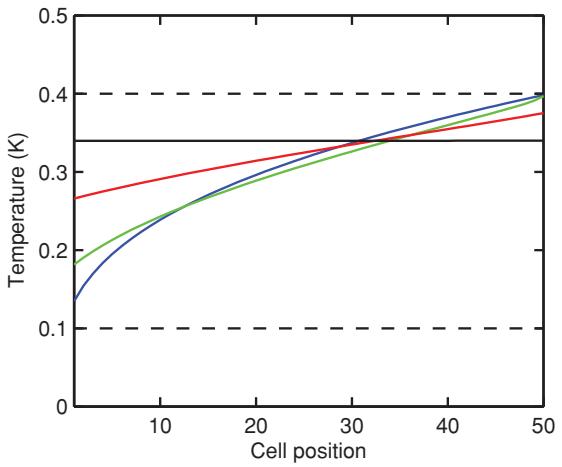

FIG. 4. (Color online) Temperature distributions of 1D microbridges terminated at $T_h = 0.4$ K and $T_c = 0.1$ K (shown dashed). The attenuation is that of two level systems. The power attenuation factors (top to bottom on the RHS) are 6.02, 0.1, 0.01, and 4.3×10^{-6} dB GHz^{-1} per cell.

TABLE I. Simulated heat flow parameters k, in pW K^{-n}, and n, for 3D, 2D, and 1D transport, of three devices having width w, thickness t, and length l. T_{3D}-T_{2D} and T_{2D}-T_{1D} are the calculated transition temperatures based on Eq. (25). Typical values measured at 120 mK are also listed.[23–26,32]

	Device 1	Device 2	Device 3
w (μm)	2.0	2.0	1.0
t (μm)	0.5	0.2	0.2
l (μm)	500	500	500
T_{3D}-T_{2D} (K)	0.19	0.47	0.47
T_{2D}-T_{1D} (K)	0.047	0.047	0.095
k (3D)	4.9	1.9	0.6
n (3D)	2.9	2.5	1.8
k (2D)	1.5	1.5	0.7
n (2D)	2.0	2.0	1.8
k (1D)	0.3	0.3	0.3
n (1D)	1.6	1.6	1.6
k (measured)	2.0	0.75	0.25
n (measured)	3.0	1.80	1.60

As discussed in Sec. II, measurements on very thin microbridges, $t = 0.2$ μm, show exponents much smaller than $n = 2$ at low temperatures. After many simulations, we have concluded that this behavior can be most easily achieved by having an acoustic loss that increases with frequency, and that is either independent or increases with temperature, which is consistent with the known acoustic properties of amorphous dielectrics. To investigate the trends, we performed simulations using the parametric expression (20), with $a = 0.0$ and $b = 1.0$, a loss of 0.1 dB per cell at the reference frequency $f_c = 1.0$ GHz, and the saturation term suppressed. For each of three geometries a simulation was carried out for perfect 3D, 2D, and 1D transport, as defined by Eqs. (23) and (24). Values of k and n derived from fits to the simulated data are listed in Table I. The sample length l given in Table I is based on assuming that the loss in Si_xN_y at 1 GHz, and low temperature, is approximately 10 dB mm^{-1}.

Table I also lists the expected T_{3D}-T_{2D} and T_{2D}-T_{1D} transition temperatures based on Eq. (25). Looking at the column labeled Device 1, the 3D simulation is in pleasing agreement with the values of both k and n, even though generic material parameters were used, and no attempt was made to calculate the cutoff frequencies of the modes accurately. $n = 3$ is actually the universal result discovered by Zeller and Pohl[6] for the bulk conductivity of glassy materials. Looking at the column labeled Device 2, which is for a thinner bridge, the measured values are broadly in agreement with 2D transport. Finally, looking at the Device 3 column, which is for a narrower bridge, the typical experimental values are consistent with 1D transport. It is pleasing that in each case the measured values of k are within a factor of 2 of those simulated despite the simplicity of the model. Although it is important not to over interpret these results, it is clear that for narrow thin bridges the model predicts exponents well below the 1D ballistic limit, $n < 2.0$, as seen experimentally.

A key feature of the model is that we can explore the diffusive to ballistic transition. Figure 5(a) shows the conductance of a 1D microbridge as a function of length, with $a = 0.0$ and $b = 1.0$. The length is normalized to the attenuation length at 1 GHz, which for Si_xN_y is around 800 μm. The cold temperature was held at $T_c = 100$ mK, and the hot temperature was stepped between $T_h = 400$ and $T_h = 420$ mK for the purpose of determining the differential thermal conductance. The simulations are shown as filled circles. At one extreme, the propagation is ballistic, and the conductance tends to the quantum limit associated with four modes, calculated using the hot temperature. The black line assumes a $1/l$ dependence, which accurately describes the behavior when the sample is many attenuation lengths long, and operating in the diffusive limit. Deviations from the $1/l$ dependence appear when the sample becomes shorter than about 0.5 attenuation lengths at the 1-GHz reference frequency. The change from diffusive to ballistic transport is governed by the attenuation length at low frequencies, because, as has been seen, ballistic transport is associated with a much higher flux than diffusive transport, and the low-frequency ballistic behavior dominates as soon as an appreciable number of low-frequency phonons remain unscattered.

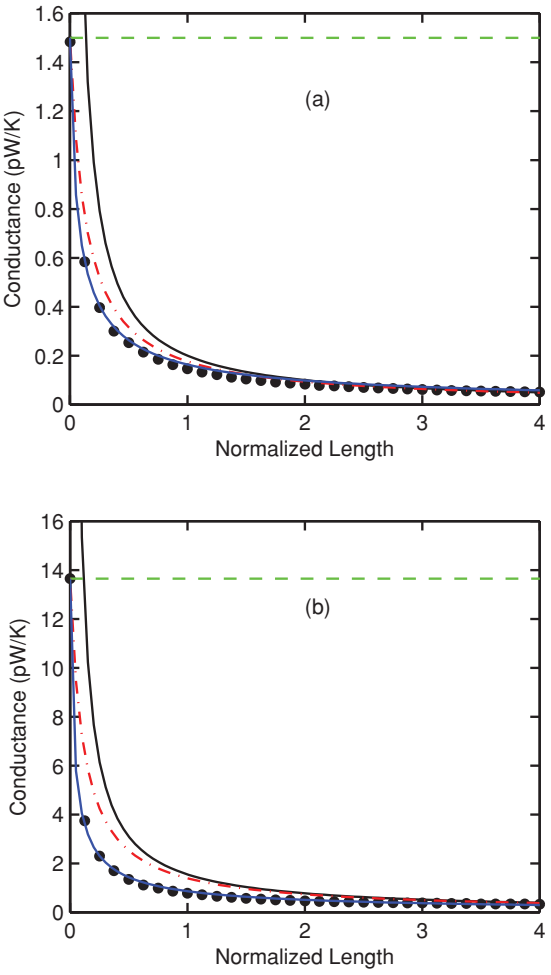

FIG. 5. (Color online) (a) 1D and (b) 2D thermal conductance as a function of sample length. The length is given in terms of the number of attenuation lengths at 1 GHz. The points show simulated results, the dashed line is the quantum limit at 0.4 K, and the solid line shows how the conductance would vary if it had a $1/l$ dependence. The dashed-dotted lines and the solid lines that pass through all of the points are the approximations described in the text.

Figure 5(b) shows the conductance of a 2D microbridge as a function of length. In this case, $w = 2$ μm, with all other parameters being the same. Assuming an acoustic attenuation factor of 10 dB mm^{-1}, the effects of ballistic transport start to become apparent for physical lengths of about 400 μm. The microbridges used for transition edge sensors are typically 100–500 μm long, and therefore they seem to be operating in the diffusive to ballistic transition. Interestingly, this observation suggests that the thermal conductance of a typical Si_xN_y microbridge could be reduced by using patterned phononic filters, even though some fraction of the transport is diffusive.

For a single-mode system, at a single frequency, in the high-occupancy limit, it can be shown analytically that the quantum-limiting behavior can be described by including a single quantum conductance in series with the conductance that would be derived on the basis of an infinitely long sample operating in the diffusive limit. In other words,

$$\frac{1}{G} = \frac{1}{G_q} + \frac{1}{G_s/l}, \tag{29}$$

where G is the overall conductance, G_q is the quantum limit, and G_s is the conductance of a unit-length section of an infinitely long sample. This behavior occurs because the overall system can be regarded as comprising a number of distinct cells, each an attenuation length long, exchanging power locally in a ballistic manner. As the physical length is reduced well below the acoustic attenuation length, the only cells remaining are the hot and cold terminations. This same model is shown in Figs. 5(a) and 5(b) as a dashed-dotted line, even though, now, a number of frequencies, having different attenuation lengths, and modes are involved. In this case it is necessary to replace G_q with the multimode quantum limit G_{ql} of the particular sample. This simple model is reasonable, but for general microbridges we find that

$$G = \left[\frac{1}{G_o} + \left(\frac{\alpha}{l}\right)^{-\beta}\right]^{-1}, \tag{30}$$

where α and β are parameters, and $\beta \sim 0.8$, provides a better description of behavior over the diffusive to ballistic transition, even for wide, thick samples. The solid lines that pass through the points in Figs. 5(a) and 5(b) show Eq. (30) with $\alpha = 0.12$ and $\alpha = 0.9$, respectively, and $\beta = 0.8$ in both cases. Interestingly, from the intercept on the $l = 0$ axis, we can derive an effective number of modes. Looking at Fig. 5(b), taking the intercept to be 14 pW K^{-1}, and dividing by the quantum conductance of a single mode, we find that approximately 37 modes are involved in the transport. It is apparent that it would be possible to determine the effective attenuation length experimentally by measuring the thermal conductance as a function of length. An important question is whether the model can describe, with a single set of parameters, the complete range of behavior seen. To make progress we must introduce modal spectra, which could be achieved by using the elastic wave equation to calculate the

cutoff frequencies of the compression, torsion, shear, and flexure waves. In a later paper we will carry out this analysis, and provide a detailed comparison with experimental data. The purpose of this paper, however, is to demonstrate how inelastic scattering can be introduced into an acoustic-wave model, and therefore we simply add up the number of cells in k space numerically. We took the size of the cells in the two Cartesian directions to be π/t and π/w, and calculated separately the number of propagating transverse n_t and longitudinal modes n_l for a given frequency using the transverse and longitudinal sound speeds. The total number of modes was then determined by $N(\omega) = 2n_t + n_l + 1$, where the factor of 2 comes from the degeneracy of the transverse modes, and the addition of 1 is needed to make up the four modes that can propagate as the frequency tends to zero. This approach is only approximate, but is in close agreement with full calculations, and matches well the 2D and 3D forms of Eqs. (23) and (24). It ignores out-of-plane flexure, because it incorrectly predicts a loss of one polarization when the corresponding bridge dimension becomes smaller than half a wavelength. An excellent description of the various modes is given by Cross and Lifshitz.[12] Here, the Debye approach is convenient and adequate because it provides a simple parametrization of when the dimensionality changes, an effect that is seen in experimental data. Also, because other numerical aspects of the model, such as the magnitude, frequency dependence, and saturation of the acoustic loss are poorly known, it provides an adequate starting point. Also, in a real experiment, issues arise as to what temperature one is actually measuring.[43]

Figure 6 shows the number of propagating modes $N(\omega)$ as a function of frequency for three different microbridge geometries: (a) $w = 4$ μm, $t = 0.5$ μm; (b) $w = 4$ μm, $t = 0.2$ μm; (c) $w = 1$ μm, $t = 0.2$ μm. In each case, there is an initial region where only four modes propagate (1D) (the very bottom of the curves), then there is a linear region corresponding to an increase in modes along the largest dimension (2D), and then the overall quadratic behavior, made up of near-piecewise linear sections, characteristic of 3D transport dominates. Certain features, for example, the discontinuity in curve (b) at 26 GHz, mark the onset of longitudinal modes, which have a different phase velocity than the transverse modes. Note that the width of the membrane determines the transition from 1D to 2D transport, whereas the thickness of the membrane determines the transition from 2D to 3D transport. Crucially, the rate of increase of the number of modes in the 2D region is determined by the width. Curves (b) and (c) show 2D behavior at frequencies of up to 15 GHz, but the rate of increase in the first linear region of (b) is much greater than that of (c). In fact, we would expect the differences in behavior between the 2D and 1D cases of (c) to be small.

The black lines in Fig. 6 show the power spectra of heat baths at 100, 200, 300, and 400 mK (left to right). Each unit of the scale corresponds to 10 aW GHz^{-1}. For curve (c), true 1D transport only takes place at frequencies below 3 GHz, corresponding to temperatures below 50 mK. For temperatures of up to 200 mK, however, the transport is nearly 1D, with the number of available modes increasing only slowly with temperature. Beyond 200 mK, the overall quadratic form dominates on the scale size of the Plank curves. In the case of curve (c), the transitions from 1D-2D-3D are more clear, but

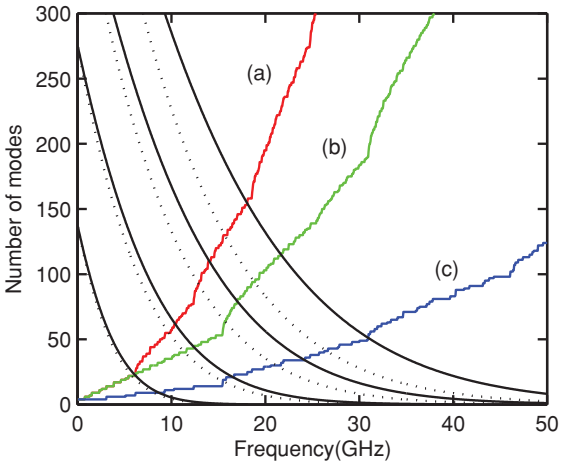

FIG. 6. (Color online) The stepped solid lines show the number of propagating modes $N(\omega)$ as a function of frequency for microbridges having dimensions (a) 4 μm wide and 0.5 μm thick, (b) 4 μm wide and 0.2 μm thick, and (c) 1 μm wide and 0.2 μm thick. The smooth solid lines show the power spectral densities, in units of 10 aW GHz^{-1}, of heat baths having temperatures (left to right) of 0.1, 0.2, 0.3, 0.4 K. The smooth dotted lines show the same power spectral densities, but with an acoustic attenuation of 0.1 dB, at the reference frequency of 1 GHz, which increases linearly with frequency.

the rate of increase of modes in the 2D region is high. Finally, in case (a), quadratic behavior becomes significant at 100 mK. The actual behavior is a smooth, weighted average over the Planck curve and the number of modes propagating at each frequency.

Figure 7 shows the heat flux as a function of temperature T_h with $T_c = 100$ mK, for a microbridge measuring 1 μm wide and 0.2 μm thick, which corresponds to curve (c) in Fig. 6. The attenuation factor was set to $\eta = 4.3 \times 10^{-6}$ dB per cell at 1 GHz to ensure ballistic transport. The dashed lines in

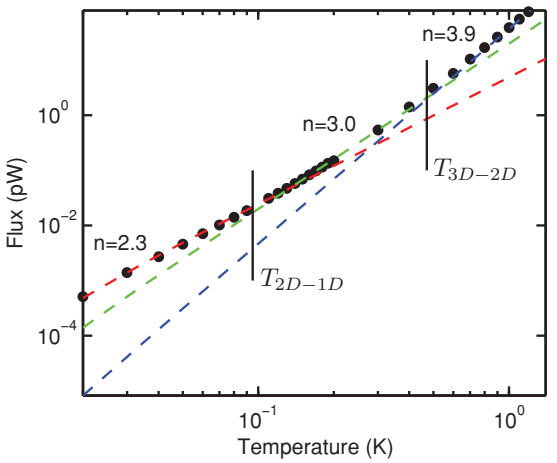

FIG. 7. (Color online) Heat flux as a function of hot temperature for a microbridge measuring 1 μm wide and 0.2 μm thick. T_c was held constant at 0.01 K, and T_h was swept over the range shown. The attenuation factor was set to a low value, $\eta = 4.3 \times 10^{-6}$ dB per cell at 1 GHz, to ensure ballistic transport. The dashed lines correspond to fits to the expression $k(T_h^n - T_c^n)$, and the vertical lines mark the expected T_{3D}-T_{2D} and T_{2D}-T_{1D} transition temperatures.

Fig. 7 correspond to power-law fits to the regions where 3D, 2D, and 1D transport might be expected to dominate. For each of the regions we find (3D) $k = 37.0$, $n = 3.9$; (2D) $k = 20.0$, $n = 3.0$; and (1D) $k = 4.9$, $n = 2.3$. On inspection of Fig. 6, it can be seen that perfect 1D behavior is never realized even at 20 mK because the Planck spectrum smears the 1D-2D transition. A key point about Fig. 7 is that the change in slope seems to indicate 1D to 3D behavior, with the 2D behavior being almost lost in the general curvature of the transition. This feature is characteristic of experimental data. The vertical black lines, however, show the expected transition temperatures calculated on the basis of Eq. (25), and they correspond to the intercepts of the power-law fits.

Figure 6 also shows, as dashed lines, the Planck curves attenuated by a loss having $\eta^m(T_c,\omega_c) = 0.1$ dB, $a = 0$, $b = 1.0$, and $\omega_c = 1$ GHz. Figure 8 shows the corresponding flux as a function of temperature for a microbridge having $w = 1$ μm and $t = 0.2$ μm. Figure 8 should be compared with the equivalent lossless case of Fig. 7. Notice that the dimensionality of the transport changes at higher temperatures compared with the ballistic case, as would be expected on the basis of Fig. 6, and the transitions from 1D to 2D and 2D to 3D transport are less well defined. In the lossy case, the low-temperature exponent is reduced to $n = 1.8$, and the high-temperature exponent to $n = 2.9$, shown as dashed lines. The low-temperature exponent is fully consistent with typical values measured, the intermediate-temperature exponent is characteristic of the bulk behavior of amorphous materials, but the high-temperature exponent is much too small. In addition, using the same loss, we modeled a sample having $w = 10$ μm and $t = 0.5$ μm, and found the low- and high-temperature exponents to be $n = 2.4$ and $n = 2.9$, respectively. These contrast with experimental values of $n = 1.8$ at 0.27 K changing smoothly to $n = 3.6$ at 1.5 K. The simulated low-temperature exponent could be reduced further, but only at the expense of reducing the high-temperature exponent. We performed many simulations, using the parametric expression for the losses [Eq. (20)] and the form appropriate for TLSs [Eq. (17)], and were always left with the problem that the low-temperature exponent n could not be reduced to the range of values measured without reducing the high-temperature exponent significantly below the range of values measured. The discrepancy is very marked, and is an inevitable consequence of having an acoustic attenuation that increases with frequency, whatever the precise physical origin. A similar problem occurs with elastic scattering, as commented on by other authors, but in the case of inelastic scattering there is a possible explanation.

It is well known that acoustic loss in amorphous dielectrics at low temperatures decreases as the wave amplitude exceeds some critical value, Eq. (20); a process known as saturation. Because the acoustic loss is a function of both flux and temperature, the root finding algorithm must find the flux that not only leads to thermal equilibrium but also gives the correct loss at each position. We have found that Eq. (28) converges satisfactorily as long as the solution of the last calculation is used as the starting guess of the next calculation as the temperature of the hot termination is varied.

Figure 9 shows the flux as a function of temperature for a microbridge having $w = 1$ μm and $t = 0.2$ μm. The loss was made dependent on the square of the frequency, $b = 2.0$, having a value of 0.2 dB per cell at the reference frequency 1 GHz. The lower curve corresponds to the case where there is no saturation, and the top curve to the case where the loss saturates at a heat flux of $I_s = 6$ fW, which is characteristic of glassy materials.[33,36]. For the lower curve, $n = 1.5$ at low temperatures and $n = 2.8$ at high temperatures. Thus, as already described, a reduction in n below the 1D ballistic value can only be achieved at the expense of reducing n at high temperatures. The top curve, however, has $n = 1.7$ at low temperatures, and $n = 4.0$ at high temperatures. Therefore, the low-temperature exponent can be suppressed significantly without reducing the high-temperature value. A series of simulations were carried out using saturation fluxes over the

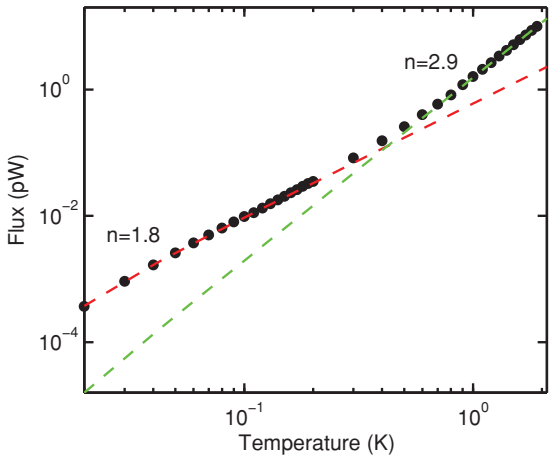

FIG. 8. (Color online) Heat flux as a function of hot temperature T_h for a bridge measuring 1 μm wide and 0.2 μm thick. T_c was held constant at 0.01 K. The attenuation factor was set to $\eta = 0.1$ dB per cell at 1 GHz, and increased linearly with ω. The dashed lines correspond to fits to the expression $k(T_h^n - T_c^n)$.

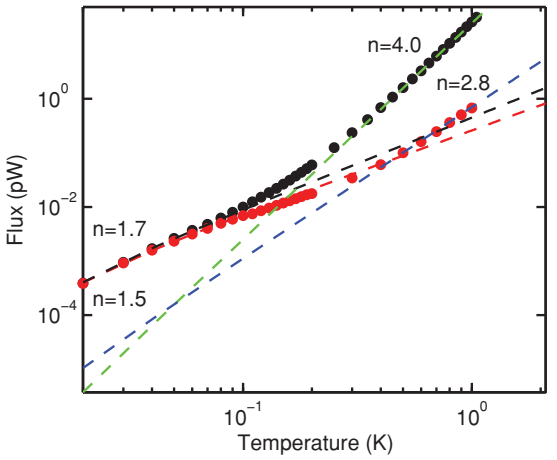

FIG. 9. (Color online) Heat flux as a function of hot temperature T_h for a bridge measuring 1 μm wide and 0.2 μm thick. T_c was held constant at 0.01 K. In this case the loss increased as ω^2, and had a value of 0.2 dB per cell at the reference frequency of 1 GHz. The top curve shows the behavior without saturation, and the bottom curve shows the behavior with a saturation flux of $I_s = 6$ fW. The dashed lines correspond to fits to the expression $k(T_h^n - T_c^n)$.

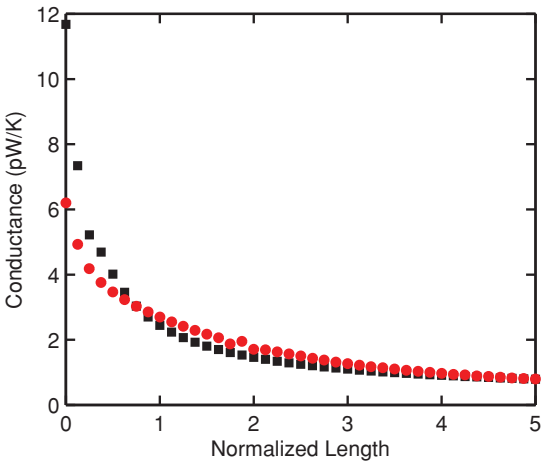

FIG. 10. (Color online) Conductance as a function of normalized length for a bridge measuring 1 μm wide and 0.2 μm thick. The squares corresponds to $T_c = 70$ and $T_h = 130$ mK, and the circles to $T_c = 70$ and $T_h = 340$ mK. The conductances of the low-temperature curve have been scaled by a factor of 12 to allow comparison.

range $I_s = 0$ to $I_s = 6$ fW, and they spanned the behavior seen in Fig. 9. Crucially, the simulations show that a sample may behave diffusively at low temperatures, but near-ballistically at high temperatures, which is counterintuitive but, qualitatively at least, in accordance with measurements.

The inclusion of saturation gives rise to a variety of unexpected phenomena, and may shed light on the peculiarities listed in Sec. II. For example, Fig. 10 shows the conductance of a sample as a function of length. The same microbridge was chosen as for Fig. 9, but in one case the simulation was carried out with $T_c = 70$ and $T_h = 130$ mK (squares), and in the other case with $T_c = 70$ and $T_h = 340$ mK (circles). The low-temperature curve has been scaled by a factor of 12 to allow it to be plotted on the same graph as the high-temperature curve. For Si_xN_y, a normalized length of 1.0 corresponds to about 800 μm. Notice that with a small temperature difference, the sample behaves in a diffusive manner, showing a near-$1/l$ dependence over the range of lengths typically used, 200–1200 μm, but with a high temperature difference, the same sample behaves in a ballistic manner, showing strong evidence for a finite intercept at $l = 0$. We have seen this behavior in measurements on samples of this size, and it is highly suggestive of a saturating inelastic scattering process. Finally, using the single-mode quantum conductance, and the intercepts, we can calculate the effective number of modes for the two curves shown in Fig. 10; we find $n = 19$ for the high-temperature measurement, and $n = 8$ for the low-temperature measurement. Using the same analysis method on experimental data from a bridge having these dimensions, we find $n = 19$ for the high-temperature measurement, which is in pleasing agreement given the simplicity of the model.

VI. CONCLUSIONS

We have discussed, and emphasized, the role of acoustic loss in influencing the low-temperature thermal conductance of amorphous dielectric microbridges. A model has been devised that allows behavior to be simulated in the diffusive to ballistic transition. Transport will tend to be ballistic at long wavelengths, but diffusive at short wavelengths, with ballistic transport becoming increasingly apparent as the length of a sample is made sufficiently small that an appreciable number of low-energy phonons remain unscattered. In Si_xN_y, deviations should start to appear at about 400 μm, which is typical of the lengths used for micromachined components, such as transition edge sensors. The model can accommodate a wide range of functional forms for acoustic loss, and it gives not only the thermal flux as a function of geometry and temperature but also the temperature distribution of the internal degrees of freedom that constitute the loss, which in turn can be used for calculating noise. The model reproduces all of the features characteristic of low-temperature thermal transport, and provides a conceptually appealing numerical framework for interpreting experimental data. Although no attempt has been made to fit experimental data precisely, which will be the subject of a later paper, the model gives fluxes and conductances that are within of a few of those measured, and produces temperature dependencies typical of those seen.

It is possible to include flux-dependent acoustic loss, and thereby model saturation, which has been shown to lead to counterintuitive thermal behavior. Crucially, a sample can behave diffusively when measured using a small temperature difference, but ballistically when measured using a large temperature difference. There is much circumstantial evidence that the effects of saturation have been seen, but not explicitly recognized, on many occasions; and if confirmed, this observation would have significant implications for the design of ultra-low-noise TESs. For example, it may be beneficial, from the point of view of both small signal and noise behavior, to operate TESs with the largest possible temperature differences (by keeping the bath temperature low) to ensure that the losses are saturated. A particularly revealing experiment would be to measure the thermal conductance of a TES while applying a variable-frequency microwave electromagnetic field to the legs, perhaps by making the legs the dielectric of a superconducting microstrip transmission line. The relationship between the acoustic and electric properties of the material[36] would suggest that the behavior of the TES could be influenced by passing low levels (< 80 dBm) of microwave power through the transmission line.

The opportunities for further study are considerable. For example, it would be straightforward to allow heat flow in a plane, and to include inelastic scattering, representing, say, surface roughness. Our ambition is to set up a general model based on mode matching at discontinuities, cascaded scattering matrices, and the power-balance method described here, to allow patterned microbridges, having, say, stepped widths, to be simulated. We would then be in a position to model the behavior of phononic thermal filters operating in the ballistic to diffusive transition, opening up a range of new design opportunities. Such an extension would show the smooth way in which a filter changes from displaying strong interference effects to behaving in a simple diffusive manner as the key longitudinal dimensions are made larger than the low-frequency scattering length.

*stafford@mrao.cam.ac.uk

[1] F. Giazotto, T. T. Heikkilä, A. Luukanen, A. M. Savin, and J. P. Pekola, Rev. Mod. Phys. **78**, 217 (2006).

[2] L. G. C. Rego and G. Kirczenow, Phys. Rev. Lett. **81**, 232 (1998).

[3] K. D. Irwin and G. C. Hilton, in *Cryogenic Particle Detection*, edited by C. Enss, Topics of Applied Physics, Vol. 99 (Springer, Berlin, 2005), p. 63.

[4] T. Kühn, D. V. Anghel, J. P. Pekola, M. Manninen, and Y. M. Galperin, Phys. Rev. B **70**, 125425 (2004).

[5] H. B. G. Casimir, Physica **5**, 495 (1938).

[6] R. C. Zeller and R. O. Pohl, Phys. Rev. B **4**, 2029 (1971).

[7] P. W. Anderson, B. I. Halperin, and C. M. Varma, Philos. Mag. **25**, 1 (1971).

[8] K. Y. Yasumura, T. D. Stowe, E. M. Chow, T. Pfafman, T. W. Kenny, B. C. Stipe, and D. Rugar, J. Micromechan. Syst. **9**, 117 (2000).

[9] W. A. Phillips, J. Low Temp. Phys. **7**, 351 (1972).

[10] N. Nishiguchi, Y. Ando, and M. N. Wybourne, J. Phys. Condens. Matter **9**, 5751 (1997).

[11] D. H. Santamore and M. C. Cross, Phys. Rev. B **66**, 144302 (2002).

[12] M. C. Cross and R. Lifshitz, Phys. Rev. B **64**, 085324 (2001).

[13] K. Schwab, E. A. Henriksen, J. M. Worlock, and M. L. Roukes, Nature (London) **404**, 974 (2000).

[14] B. A. Glavin, Phys. Rev. Lett. **86**, 4318 (2001).

[15] W. Arnold and S. Hunklinger, Solid State Commun. **17**, 883 (1975).

[16] M. von Schickfus and S. Hunklinger, J. Phys. C **9**, L439 (1976).

[17] M. von. Schickfus, S. Hunklinger, and L. Piché, Phys. Rev. Lett. **35**, 876 (1975).

[18] T. Kühn, D. V. Anghel, Y. M. Galperin, and M. Manninen, Phys. Rev. B **76**, 165425 (2007).

[19] D. V. Anghel, T. Kühn, Y. M. Galperin, and M. Manninen, Phys. Rev. B **75**, 064202 (2007).

[20] M. Von Haumeder, U. Strom, and S. Hunklinger, Phys. Rev. Lett. **44**, 84 (1980).

[21] S. Hunklinger, J. Phys. Colloques **43**, C9-461 (1982).

[22] J. L. Black, Phys. Rev. B **17**, 2740 (1978).

[23] K. Rostem, D. Glowacka, D. J. Goldie, and S. Withington, J. Low Temp. Phys. **151**, 76 (2008).

[24] K. Rostem, D. M. Glowacka, D. J. Goldie, and S. Withington, in *Millimeter and Submillimeter Detectors and Instrumentation for Astronomy IV*, Proc. SPIE, Vol. 7020 (SPIE, Bellingham, WA, 2008).

[25] K. Rostem, D. J. Goldie, S. Withington, D. M. Glowacka, V. N. Tsaneva, and M. D. Audley, J. Appl. Phys. **105**, 084509 (2009).

[26] D. J. Goldie, A. V. Velichko, D. M. Glowacka, and S. Withington, J. Appl. Phys. **109**, 083105 (2011).

[27] M. M. Leivo and J. P. Pekola, Appl. Phys. Lett. **72**, 1305 (1998).

[28] W. Holmes, J. M. Gildemeister, and P. L. Richards, Appl. Phys. Lett. **72**, 2250 (1998).

[29] C. S. Yung, D. R. Schmidt, and A. N. Cleland, Appl. Phys. Lett. **81**, 31 (2002).

[30] B. L. Zink and F. Hellman, Solid State Commun. **129**, 199 (2004).

[31] H. F. C. Hoevers, M. L. Ridder, A. Germeau, M. P. Bruijn, P. A. J. de Korte, and R. J. Wiegerink, Appl. Phys. Lett. **86**, 251903 (2005).

[32] D. J. Goldie, D. M. Glowacka, K. Rostem, and S. Withington, in Proceedings of the 21st International Symposium on Space Terahertz Technology, Oxford, 2010 (unpublished) [http://go.nrao.edu/ISSTT].

[33] B. Golding, J. E. Graebner, and R. J. Schutz, Phys. Rev. B **14**, 1660 (1976).

[34] C. C. Yu and J. J. Freeman, Phys. Rev. B **36**, 7620 (1987).

[35] M. Durandurdu and D. A. Drabold, Phy. Rev. B **66**, 155205 (2002).

[36] C. Laermans, W. Arnold, and S. Hunklinger, J. Phys. C **10**, L161 (1977).

[37] G. Frossati, J. le G. Gilchrist, J. C. Lasjaunias, and W. Meyer, J. Phys. C **10**, L515 (1977).

[38] M. Modest, *Radiative Heat Transfer* (McGraw Hill, New York, 1993).

[39] T. Klitsner, J. E. VanCleve, H. E. Fischer, and R. O. Pohl, Phys. Rev. B **38**, 7576 (1988).

[40] A. Majumdar, J. Heat Transfer **115**, 7 (1993).

[41] A. A. Joshi and A. Majumdar, J. Appl. Phys. **74**, 31 (1993).

[42] G. Chen, Phys. Rev. Lett. **86**, 2297 (2001).

[43] G. Chen, J. Heat Transfer **124**, 320 (2002).